

Effect of Nonmagnetic Substitution on the Magnetic Properties and Charge-Transfer Phase Transition of an Iron Mixed-Valence Complex, $(n\text{-C}_3\text{H}_7)_4\text{N}[\text{Fe}^{\text{II}}\text{Fe}^{\text{III}}(\text{dto})_3]$ ($\text{dto} = \text{C}_2\text{O}_2\text{S}_2$)

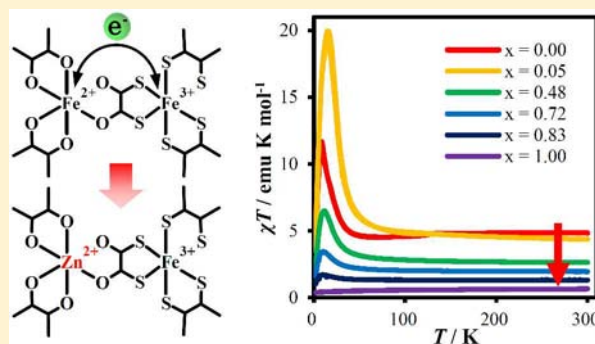
Hiromichi Ida,[†] Atsushi Okazawa,[‡] Norimichi Kojima,[‡] Ryo Shimizu,[†] Yasuhiro Yamada,[†] and Masaya Enomoto^{*†}

[†]Department of Chemical Science and Technology, Graduate School of Chemical Science and Technology, Tokyo University of Science, Kagurazaka 1-3, Shinjuku-ku, Tokyo 162-8601, Japan

[‡]Department of Basic Science, Graduate School of Arts and Sciences, The University of Tokyo, Komaba 3-8-1, Meguro-ku, Tokyo 153-8902, Japan

Supporting Information

ABSTRACT: The iron mixed-valence complex $(n\text{-C}_3\text{H}_7)_4\text{N}[\text{Fe}^{\text{II}}\text{Fe}^{\text{III}}(\text{dto})_3]$ exhibits a novel type of phase transition called charge-transfer phase transition (CTPT), where the thermally induced electron transfer between Fe^{II} and Fe^{III} occurs reversibly at ~ 120 K, in addition to the ferromagnetic phase transition at $T_C = 7$ K. To investigate the mechanism of the CTPT, we have synthesized a series of magnetically diluted complexes $(n\text{-C}_3\text{H}_7)_4\text{N}[\text{Fe}^{\text{II}}_{1-x}\text{Zn}^{\text{II}}_x\text{Fe}^{\text{III}}(\text{dto})_3]$ ($\text{dto} = \text{C}_2\text{O}_2\text{S}_2$; $x = 0\text{--}1$), and carried out magnetic susceptibility and dielectric constant measurements and ^{57}Fe Mössbauer spectroscopy. With increasing Zn^{II} concentration (x), the CTPT is gradually suppressed and disappears at $x \approx 0.13$. On the other hand, the ferromagnetic transition temperature (T_C) is initially enhanced from 7 K to 12 K between $x = 0.00$ and 0.05, despite the nonmagnetic nature of Zn^{II} ions, and then it decreases monotonically from 12 K to 3 K with increasing Zn^{II} concentration. This anomalous dependence of T_C on Zn^{II} concentration is related to a change in the spin configuration of the ferromagnetic state caused by the partial suppression of the CTPT.



INTRODUCTION

In the past few decades, there has been a growing interest in molecule-based magnetic materials. The versatility and flexibility of molecular chemistry provide a possibility of fine-tuning the nuclearity, structure, and magnetic dimensionality, which makes it possible to design novel magnetic materials, such as single-molecule magnets (SMMs^{1–4}) and single-chain magnets (SCMs^{5–8}). Another important topic in this field is the creation of multifunctional magnets. Materials in this class possess one or more additional functionalities, along with a magnetic property within a single compound, which leads to a unique opportunity for interplay between these properties to generate novel functional materials, such as metallic magnets,^{9–11} proton-conducting magnets,^{12–14} superconducting magnets,^{15,16} and photocontrollable magnets.^{17–22}

Among various ligands, oxalate dianion (ox) attracts much attention, because of its ability to bridge two metal ions, generally in the bis-bidentate mode, and mediates a strong magnetic interaction between them. To construct an oxalato-complex with a particular magnetic dimensionality, a tris-oxalato complex $[\text{M}^{\text{III}}(\text{ox})_3]^{3-}$ (M^{III} = trivalent transition-metal ion) is widely used as the metal-containing ligand bridges several metal ions to construct homometallic and hetero-

metallic multinuclear complexes with wide ranges of structure and dimensionality. In this family, the bimetallic anionic complexes $[\text{M}^{\text{II}}\text{M}^{\text{III}}(\text{ox})_3]^-$ (M^{II} = Mn, Fe, Co, Ni, Cu, Zn; M^{III} = Cr, Fe, Ru, V, Mn) have been extensively investigated since the discovery of ferromagnetic ordering in the oxalato-bridged bimetallic layered complexes $(n\text{-C}_4\text{H}_9)_4\text{N}[\text{M}^{\text{II}}\text{Cr}^{\text{III}}(\text{ox})_3]$ (M = Mn, Cr, Fe, Co, Ni, Cu).²³ These complexes exhibit two-dimensional (2D) or three-dimensional (3D) architecture, depending on the size, charge, and geometry of the counteranion that templates the formation of the anionic bimetallic network.²⁴ The 2D structural complexes are obtained when a bulky tetraalkylammonium cation $(n\text{-C}_n\text{H}_{2n+1})_4\text{N}^+$ ($n = 3\text{--}6$) is used as a template cation.^{23,25–29} Furthermore, the alkylammonium cation can be substituted with an organic or organometallic cation having various functionalities, such as a paramagnetic cation,^{30–32} photochromic cation,³³ conductive cation,^{9,34,35} proton-conducting cation,¹² nonlinear optical active cation,^{36–38} or molecular rotor cation.³⁹ Thus the ox-bridged bimetallic complex system $\text{A}[\text{M}^{\text{II}}\text{M}^{\text{III}}(\text{ox})_3]$ (A = cation) possesses ferromagnetic, antiferromagnetic, or ferri-

Received: May 25, 2012

Published: August 6, 2012

magnetic ordering, together with additional functionality arising from the substituent cation.

On the other hand, ox can also be substituted by the 1,2-dithiooxalato dianion (dto) to form a similar 2D bimetallic anionic network, which was first reported for $(n-C_nH_{2n+1})_4N[M^{II}Cr^{III}(dto)_3]$ ($M = Fe, Co, Ni, Zn$).⁴⁰ Among this family, the iron mixed-valence complexes, $(n-C_nH_{2n+1})_4N[Fe^{II}Fe^{III}(dto)_3]$ ($n = 3, 4$) exhibit a novel type of phase transition called charge-transfer phase transition (CTPT), where the thermally induced charge transfer (CT) between Fe^{II} and Fe^{III} occurs reversibly, as shown schematically in Figure 1.^{41–43} In the case of (n -

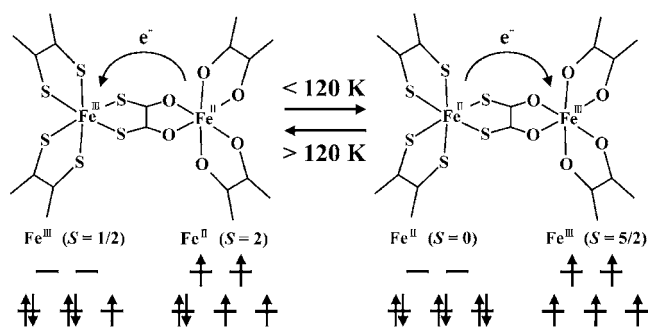


Figure 1. Schematic representation of the charge-transfer phase transition (CTPT) in $(n-C_3H_7)_4N[Fe^{II}Fe^{III}(dto)_3]$.

$C_3H_7)_4N[Fe^{II}Fe^{III}(dto)_3]$ at room temperature, Fe^{III} in the low-spin state is coordinated by six S atoms of the dto, while Fe^{II} in the high-spin state is coordinated by six O atoms. The phase with this spin configuration, $Fe^{II}(S = 2)–Fe^{III}(S = 1/2)$, is denoted as the high-temperature phase (HTP). At ~ 120 K, the CTPT occurs with a one-electron transfer from Fe^{II} to Fe^{III} sites. As a result of this phase transition, the spin configuration changes from the HTP to the low-temperature phase (LTP), where Fe^{II} site surrounded by S atoms is in the low-spin state, while Fe^{III} site surrounded by O atoms is in the high-spin state, i.e., $Fe^{II}(S = 0)–Fe^{III}(S = 5/2)$. In contrast to $(n-C_nH_{2n+1})_4N[Fe^{II}Fe^{III}(dto)_3]$ with $n = 3$ and 4, no CTPT is observed for $(n-C_nH_{2n+1})_4N[Fe^{II}Fe^{III}(dto)_3]$ with $n = 5$ and 6; hence, the spin configuration of these complexes remain in the HTP over the entire measurement temperature range between 300 K and 2 K.⁴⁴ In addition to the CTPT, the ferromagnetic transition for the LTP spin state is observed at $T_C = 7$ K for $(n-C_3H_7)_4N[Fe^{II}Fe^{III}(dto)_3]$, while that for the HTP spin state is observed at 19.5 K for $(n-C_5H_{11})_4N[Fe^{II}Fe^{III}(dto)_3]$. This result shows that the spin configuration of the HTP gives a higher T_C value than that of the LTP; thus, the ferromagnetic transition of the iron mixed-valence complex $[Fe^{II}Fe^{III}(dto)_3]^-$ can be controlled by the size of the intercalated cation.²⁰

The dielectric response associated with electron transfer between metal sites has been reported for some of the biferrrocenium-based CT salts. In the cases of $1',1'''$ -didodecylbiferrrocenium triiodide⁴⁵ and $(1',1'''$ -isopropyl-1,1''-biferrrocene) $[Ni(mnt)_2]$,⁴⁶ an enhancement of the dielectric constant without frequency dependence is observed, which is attributed to a rapid valence tautomerization accompanied by a polarity inversion of the biferrrocenium-based cation. These complexes exhibit a valence detrapped–trapped transition, and the electron transfer is gradually frozen below the transition temperature, which results in a decrease in the dielectric constant with decreasing temperature. These facts suggest that the dielectric measurement is valuable to observe the CT

phenomena between metal sites in a CT complex. In the case of $(n-C_3H_7)_4N[Fe^{II}Fe^{III}(dto)_3]$, it has been reported that the nature of the CT in the CTPT is the oscillation of electrons between Fe^{II} and Fe^{III} with dynamic fluctuation of the internal field.⁴⁷ Therefore, it is expected that an anomalous enhancement of the dielectric constant will be observed associated with the CTPT, which can thus be detected by means of dielectric measurement.

Recently, we have synthesized the magnetically diluted complexes $(n-C_3H_7)_4N[Fe^{II}_{1-x}Zn^xFe^{III}(dto)_3]$ ($x = 0–1$) to investigate the effects of magnetic dilution on the magnetic property and CTPT of $(n-C_3H_7)_4N[Fe^{II}Fe^{III}(dto)_3]$.⁴⁸ From the results of magnetic susceptibility measurements and ^{57}Fe Mössbauer spectroscopy, it was determined that the CTPT is quenched by the substitution of Fe^{II} with Zn^{II} with a critical concentration below $x = 0.26$. The suppression of the CTPT causes an enhancement of the T_C value, despite the dilution of magnetic sites with nonmagnetic ions. With further increases in the concentration x , T_C decreases until the ferromagnetic transition almost disappears between $x = 0.96$ and 1.00. However, the detailed concentration dependence of the spin configuration and the magnetic behavior of this system has not yet been clear, particularly at the dilution ratio x around the critical concentration for the disappearance of the CTPT.

In this article, we report the temperature-dependent dielectric response related to the CTPT for $(n-C_3H_7)_4N[Fe^{II}Fe^{III}(dto)_3]$ at various frequencies. Furthermore, the effects of magnetic dilution on the electronic and magnetic states of $(n-C_3H_7)_4N[Fe^{II}_{1-x}Zn^xFe^{III}(dto)_3]$ ($x = 0–1$) are assessed by means of dielectric constant measurement in addition to magnetic susceptibility and Mössbauer spectroscopy. On the basis of these measurements, a magnetic phase diagram for this system and a mechanism of the CTPT are proposed.

EXPERIMENTAL SECTION

Synthesis. The precursor $KBa[Fe(dto)_3] \cdot 3H_2O$ was prepared according to the literature.⁴⁹ All other reagents and solvents were commercial-grade reagents and used without further purification.

$(n-C_3H_7)_4N[Fe^{II}_{1-x}Zn^xFe^{III}(dto)_3]$ were prepared with several Zn^{II} concentrations by a previously reported method,^{44,48} except for using the appropriate amount of $ZnCl_2$ in place of $FeCl_2 \cdot 4H_2O$. A solution containing $(n-C_3H_7)_4NBr$ (0.15 g, 0.56 mmol) and the appropriate proportion of divalent metal chlorides (total of 0.38 mmol) in a 3:2 methanol/water mixture (15.2 mL) was stirred. To this, a solution of $KBa[Fe(dto)_3] \cdot 3H_2O$ (0.246 g, 0.38 mmol) in a 3:2 methanol/water mixture was added dropwise. Black powdered sample was immediately precipitated, collected by suction filtration, and washed with a 1:1 methanol/water mixture, methanol, and ether before being dried in vacuo.

Measurements. The ratios of divalent metal ions in the diluted magnetic system were determined by JEOL Model EX-2300BU energy-dispersive X-ray spectroscopy (EDS) in a JEOL Model JSM-6700F field-emission scanning electron microscope (SEM). The powder X-ray diffractions for all samples were measured with a Rigaku multiflex diffractometer using $Cu K\alpha$ radiation at room temperature. The static magnetic susceptibilities were measured with a Quantum Design MPMS-5 SQUID susceptometer in the temperature range of 2–300 K under the static magnetic field of 5000 Oe. The magnetic susceptibility data were corrected for diamagnetic contributions using Pascal's constants. The temperature dependence of the zero-field-cooled magnetization (ZFCM) and the field-cooled magnetization (FCM) were measured in the temperature range of 2–30 K under 30 Oe. The remnant magnetization (RM) was measured in the same temperature range under zero field. ac magnetic susceptibility measurements were performed in the temperature range of 2–40 K under ac magnetic field of 3 Oe and frequency range of 10–1000 Hz.

For the ^{57}Fe Mössbauer spectroscopic measurements (Wissel Model MDU1200), ^{57}Co in Rh was used as a γ -ray source. The spectra were calibrated using the six lines of a body-centered cubic iron foil (α -Fe), the center of which was taken as zero isomer shift. The temperature dependence of the dielectric constant was measured in the temperature range of 4–300 K and the frequency range of 1 Hz to 1 MHz by the two-probe method on a pellet sample by applying carbon paste onto the two surfaces. Measurements were made using a Solartron 1260 impedance gain phase analyzer equipped with a Solartron 1269 dielectric interface.

RESULTS AND DISCUSSION

We prepared 10 compositions of mixed-metal complexes $(n\text{-C}_3\text{H}_7)_4\text{N}[\text{Fe}^{\text{II}}_{1-x}\text{Zn}^{\text{II}}_x\text{Fe}^{\text{III}}(\text{dto})_3]$ with Zn^{II} concentrations $x = 0.00, 0.05, 0.13, 0.26, 0.48, 0.62, 0.72, 0.83, 0.96,$ and 1.00 by using starting solutions with $\text{Zn}^{\text{II}}/\text{Fe}^{\text{II}}$ ratios of $0.00, 0.01, 0.02, 0.05, 0.10, 0.15, 0.20, 0.30, 0.53,$ and $1.00,$ respectively. It should be noted that $x = 0.05, 0.13, 0.62, 0.72,$ and 0.83 are complementary samples to previous literature, because the original concentration interval was too coarse to explain the concentration dependence of the magnetic properties of this system. The data of powder XRD and magnetic measurements for $x = 0.00, 0.26, 0.48, 0.96,$ and 1.00 are those already reported in the previous literature.⁴⁸ We combine these data to present a unified explanation in the below discussion.

All the complexes were characterized by powder XRD. As shown in Figure 2, the diffraction patterns of the mixed-metal

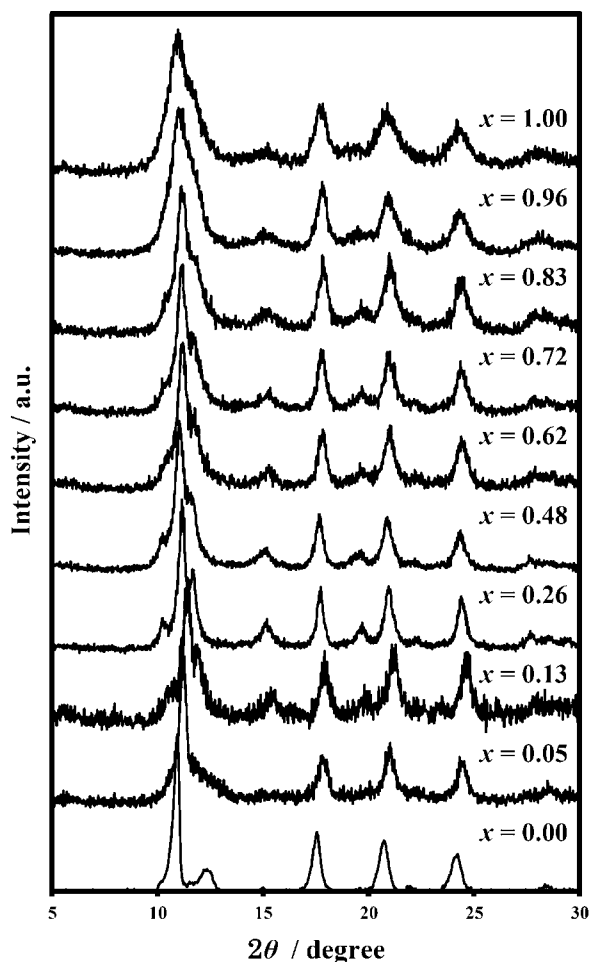


Figure 2. Powder X-ray diffraction (XRD) pattern of $(n\text{-C}_3\text{H}_7)_4\text{N}[\text{Fe}^{\text{II}}_{1-x}\text{Zn}^{\text{II}}_x\text{Fe}^{\text{III}}(\text{dto})_3]$.

complexes are similar to that previously reported for the parent complex $(n\text{-C}_3\text{H}_7)_4\text{N}[\text{Fe}^{\text{II}}\text{Fe}^{\text{III}}(\text{dto})_3]$,⁴³ indicating that the $(n\text{-C}_3\text{H}_7)_4\text{N}[\text{Fe}^{\text{II}}_{1-x}\text{Zn}^{\text{II}}_x\text{Fe}^{\text{III}}(\text{dto})_3]$ series is isostructural over the entire Zn^{II} concentration range, and thus the structure of these complexes consist of 2D honeycomb networks with alternating arrays of M^{II} ($\text{M} = \text{Zn}, \text{Fe}$) and Fe^{III} through dto bridges.

Figure 3a shows the temperature dependence of the molar magnetic susceptibility multiplied by temperature (χT) for the selected samples, $x = 0.00, 0.05, 0.48, 0.72, 0.83,$ and 1.00 to clarify the Zn^{II} concentration dependence of the magnetic property of this series. The remaining data are shown in the Supporting Information (Figure S1). At room temperature, the χT value decreases with increasing Zn^{II} concentration, which is consistent with the decrease in the effective magnetic moment per $[\text{Fe}^{\text{II}}_{1-x}\text{Zn}^{\text{II}}_x\text{Fe}^{\text{III}}(\text{dto})_3]$ unit, corresponding to the non-magnetic substitution of the Fe^{II} sites. In the low-temperature region, the χT values for the complexes with $x \leq 0.83$ increase upon cooling, reach a maximum, and then decrease. This behavior is indicative of ferromagnetic ordering within this concentration range. In contrast, the χT values gradually decrease with decreasing temperature for $x = 0.96$ and 1.00 . These results suggest that the dominant magnetic interaction in this series of complexes changes from a ferromagnetic interaction to an antiferromagnetic one between $x = 0.83$ and 0.96 . Moreover, the spin transition with thermal hysteresis that is associated with the CTPT⁴⁴ was observed for the complexes with low Zn^{II} concentration (i.e., $x \leq 0.05$), whereas it disappears at $x = 0.13$ and above (Figure 3b). This observation is indicative of the suppression of the CTPT by the substitution of Fe^{II} with Zn^{II} with a critical concentration between $x = 0.05$ and 0.13 . The slight decrease in the χT value for $x = 0.00$ at $T \approx 120$ K is corresponding to the reduction of the effective magnetic moment associated with the CTPT. Such behavior is not observed for $x = 0.05$, despite the occurrence of the CTPT. The partial suppression of the CTPT caused by substitution of Fe^{II} by Zn^{II} ion is, as discussed later, responsible for this subtle change in the effective magnetic moment.

To quantify the Zn^{II} concentration dependence of the magnetic properties of this series, the temperature dependences of the magnetic susceptibilities in the high-temperature region (i.e., $T > 150$ K for $x \leq 0.05$, $T > 50$ K for $0.13 \leq x \leq 0.83$, and $T > 100$ K for $0.96 \leq x$) were fitted with the Curie–Weiss law,

$$\chi = \frac{C}{T - \theta}$$

where C is the Curie constant and θ is the Weiss temperature. Note that the θ values are corrected for the orbital contribution of Fe^{III} ion by using temperature-dependent magnetic susceptibility of the precursor, $\text{KBa}[\text{Fe}^{\text{III}}(\text{dto})_3] \cdot 3\text{H}_2\text{O}$.⁵⁰ Figure 4 shows the effective magnetic moment μ_{eff} per $[\text{Fe}^{\text{II}}_{1-x}\text{Zn}^{\text{II}}_x\text{Fe}^{\text{III}}(\text{dto})_3]$ unit obtained using the observed Curie constant and the formula $\mu_{\text{eff}} = (8C)^{1/2}$. The value of μ_{eff} systematically decreases with increasing x , as a result of the substitution of nonmagnetic Zn^{II} for Fe^{II} . The observed μ_{eff} values are slightly larger than that expected from the sum of the magnetic moments of the two spin sites (i.e., $\mu_{\text{eff}} = \mu_{\text{Fe}(\text{III})} + (1 - x) \times \mu_{\text{Fe}(\text{II})}$); the observed effective magnetic moment for the precursor, $\text{KBa}[\text{Fe}^{\text{III}}(\text{dto})_3] \cdot 3\text{H}_2\text{O}$ is used as $\mu_{\text{Fe}(\text{III})}$ to correct the orbital contribution of Fe^{III} ion,⁵⁰ and $\mu_{\text{Fe}(\text{II})}$ is the spin-only value for high spin Fe^{II} ; see Figure 4) with $g = 2$, which is considered to be due to a g -value shift from the free electron in the anisotropic Fe^{II} ion and/or the high-spin Fe^{III} impurity caused by linkage isomerism of the dto bridge.^{41,44} The Weiss

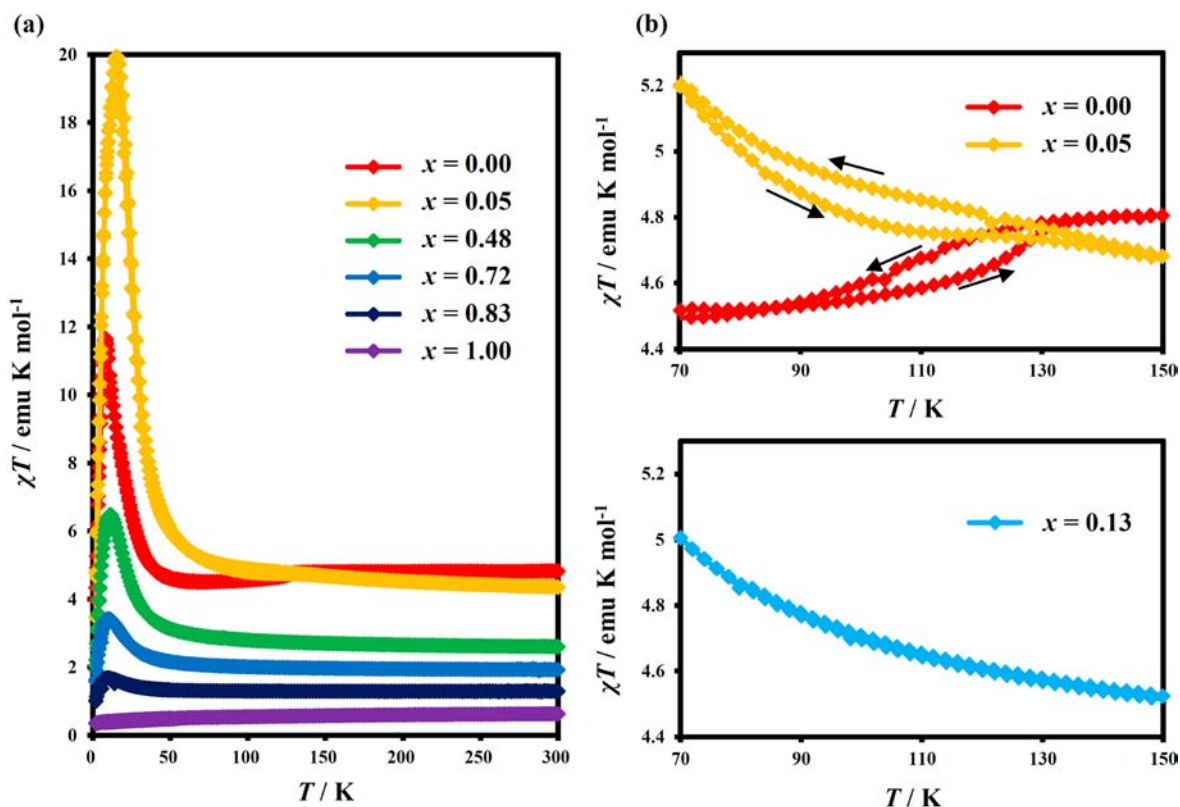


Figure 3. (a) Temperature dependence of the molar susceptibility multiplied by temperature (χT) for $x = 0.00, 0.05, 0.48, 0.72, 0.83$, and 1.00 . (b) Thermal hysteresis in the χT value corresponding to the CTPT for $x = 0.00$ and 0.05 ; hysteresis was not observed for $x = 0.13$.

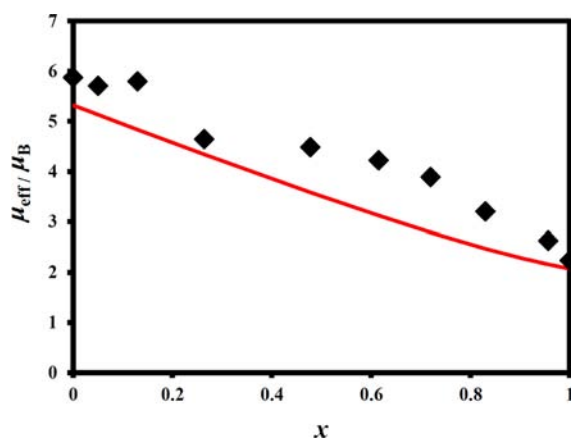


Figure 4. Variation of the effective magnetic moment (μ_{eff}) with x for $(n\text{-C}_3\text{H}_7)_4\text{N}[\text{Fe}_{1-x}\text{Zn}_x\text{Fe}^{\text{III}}(\text{dto})_3]$. The red solid line shows the effective magnetic moment expected from the sum of the magnetic moments of the two spin sites.

temperature θ gradually decreases with increasing Zn^{II} concentration at first and then abruptly decreases above $x = 0.83$, as shown in Figure 5. Such nonlinear concentration dependence of the Weiss temperature is typical for a low-dimensional magnet. It is generally expected that an absolute value of θ for a magnetic system will monotonically decrease toward zero with nonmagnetic substitution for the paramagnetic metal ion. In the present case, however, the Weiss temperature becomes zero at $x \approx 0.83$ and continues to decrease toward -17 K with increasing Zn^{II} concentration to $x = 1.00$. The ferromagnetic interaction for $(n\text{-C}_n\text{H}_{2n+1})_4\text{N}[\text{Fe}^{\text{II}}\text{Fe}^{\text{III}}(\text{dto})_3]$ ($n = 5, 6$) in the HTP is caused by the

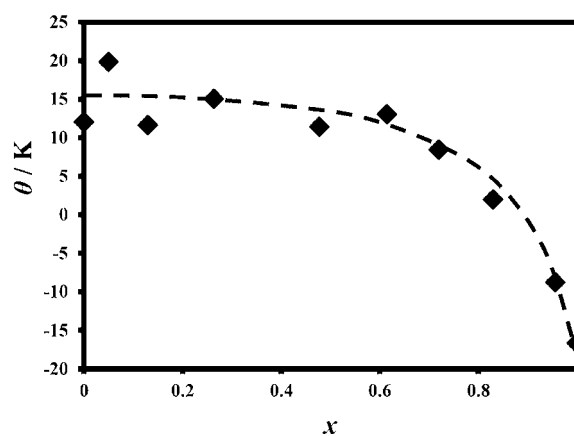


Figure 5. Variation of the Weiss temperature (θ) with x for $(n\text{-C}_3\text{H}_7)_4\text{N}[\text{Fe}_{1-x}\text{Zn}_x\text{Fe}^{\text{III}}(\text{dto})_3]$. The dashed line is a guide for the eyes.

coupling between the ground configuration $\varphi_i[\text{Fe}^{\text{III}}(t_2^5)]-\varphi_j[\text{Fe}^{\text{II}}(t_2^4e^2)]$ and the CT configuration $\varphi_i[\text{Fe}^{\text{II}}(t_2^6)]-\varphi_j[\text{Fe}^{\text{III}}(t_2^3e^2)]$, in addition to the ferromagnetic exchange interaction between Fe^{II} and Fe^{III} due to the orthogonality between the magnetic orbitals of Fe^{II} and Fe^{III} .⁴⁴ This situation is presumably similar to the case of $(n\text{-C}_3\text{H}_7)_4\text{N}[\text{Fe}_{1-x}\text{Zn}_x\text{Fe}^{\text{III}}(\text{dto})_3]$ with $x \geq 0.05$, where the ferromagnetic state is in the HTP. The nonmagnetic substitution of Fe^{II} sites with closed-shell Zn^{II} ions prevents both of these interactions, and thus θ and T_C for the HTP decrease with increasing Zn^{II} concentration. Simultaneously, this substitution creates an antiferromagnetic exchange pathway between Fe^{III} ions through the orbitals of the nonmagnetic Zn^{II} ions. The antiferromagnetic interaction compete with the ferromagnetic interaction at

$x \approx 0.83$ and the Weiss temperature θ appears to be zero. Above this Zn^{II} concentration, the antiferromagnetic interaction becomes dominant. These factors account for the strongly negative Weiss temperature for $x = 0.96$ and 1.00.

The ferromagnetic phase transition within this series of complexes was confirmed by the field-cooled magnetization (FCM), zero-field-cooled magnetization (ZFCM), and remnant magnetization (RM) measurements. The temperature dependence of the magnetization curves in the low-temperature region for the selected samples ($x = 0.00, 0.05, 0.13, 0.96,$ and 1.00) are shown in Figure 6 to show the characteristic influence of the

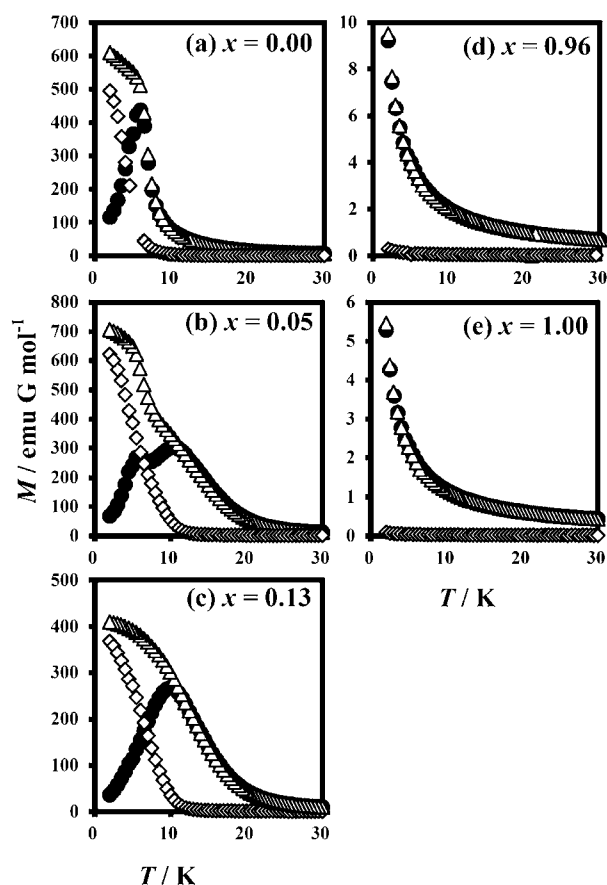


Figure 6. Temperature dependence of (Δ) the field-cooled magnetization (FCM), (\bullet) zero-field-cooled magnetization (ZFCM), and (\diamond) remnant magnetization (RM) of (a) $x = 0.00$, (b) $x = 0.05$, (c) $x = 0.13$, (d) $x = 0.96$, and (e) $x = 1.00$.

CTPT on the ferromagnetic transition. The remaining data are shown in the Supporting Information (Figure S2). For $x = 0.00$, the RM disappears at 7 K, and the FCM and ZFCM curves split below the same temperature (Figure 6a). This behavior is consistent with that previously reported for $(n\text{-C}_3\text{H}_7)_4\text{N}[\text{Fe}^{\text{II}}\text{Fe}^{\text{III}}(\text{dto})_3]$ (i.e., $x = 0.00$), which has an estimated ferromagnetic transition temperature T_C of 7 K for the LTP spin state.^{43,44} Although the T_C value for $x = 0.05$ is estimated to be 12 K from the magnetization plot (Figure 6b), in contrast to $x = 0.00$, there are two peaks in the ZFCM curve at 12 and 5.5 K and a shoulder in the FCM curve at 12 K. This behavior implies the coexistence of two ferromagnetic phases, corresponding to a HTP fragment with $T_C = 12$ K and a LTP fragment with T_C lower than that of the HTP fragment, as a result of partial suppression of the CTPT. To elucidate the ferromagnetic transition temperature for the LTP fragment in x

$= 0.05$, ac magnetic susceptibility measurements were performed (see Figure S3b in the Supporting Information). The in-phase signal (χ') shows a maximum at ~ 14 K, as well as a nonzero out-of-phase signal (χ''), which corresponds to the onset of the ferromagnetic ordering within the HTP fragment. Furthermore, an additional peak corresponding to the ferromagnetic transition within the LTP fragment appears as a shoulder at 7 K in χ' . These features clearly confirm the coexistence of two ferromagnetic phases in this compound. From these data, the ferromagnetic transition temperature for the LTP fragment in $x = 0.05$ is determined to be $T_C = 7$ K, which is the same value as T_C for the LTP in $x = 0.00$ (see Figure 6a and Figure S3a in the Supporting Information). Note that the coexistence of the two ferromagnetic phases, the HTP and LTP, is already reported for $(n\text{-C}_4\text{H}_9)_4\text{N}[\text{Fe}^{\text{II}}\text{Fe}^{\text{III}}(\text{dto})_3]$, which was confirmed by magnetic susceptibility, ^{57}Fe Mössbauer spectra, and ESR measurements.⁴⁴ As shown in Figure 6c, the peak corresponding to the LTP fragment in the ZFCM curve disappears for $x = 0.13$, which suggests that the CTPT is completely suppressed between $x = 0.05$ and 0.13. With further increases in x , the ferromagnetic transition temperature monotonically decreases and the transition almost disappears between $x = 0.96$ and 1.00 in the entire measured temperature range (see Figures 6d and 6e). The variations of T_C with x for all of the members of this series are shown in Figure 7. Generally, the ferromagnetic transition temperature

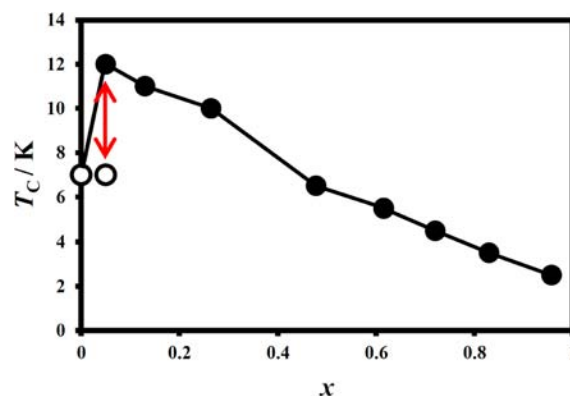


Figure 7. Variation of the ferromagnetic transition temperature (T_C) with x for $[\text{Fe}_{1-x}\text{Zn}_x\text{Fe}^{\text{III}}(\text{dto})_3]$ in the (\bullet) high-temperature phase (HTP) and (\circ) low-temperature phase (LTP). The double-headed arrow represents coexistence of the HTP and LTP.

for a diluted magnetic system decreases as the dilution ratio increases, as a result of disconnections in the exchange pathways. In the present case, however, T_C is initially enhanced between $x = 0.00$ and 0.05 and then decreases with increasing x . This anomalous behavior can be explained as follows. For $x = 0.00$, the CTPT occurs at ~ 120 K. Below this temperature, the electronic state is in the LTP. Therefore, the ferromagnetic transition for this complex occurs within the LTP. When Zn^{II} concentration is increased to $x = 0.05$, the CTPT is partially suppressed, as mentioned above; hence, the HTP fragment, whose T_C value is higher than that of the LTP fragment, remains in the low-temperature region. Note that the ferromagnetic ordering for $(n\text{-C}_3\text{H}_7)_4\text{N}[\text{Fe}^{\text{II}}\text{Fe}^{\text{III}}(\text{dto})_3]$ in the LTP is achieved by the CT interaction^{44,51} between Fe^{III} sites through nonmagnetic low-spin Fe^{II} ions. Therefore, the exchange interaction between the neighboring spin sites in the LTP is weaker than that in the HTP, and this accounts for

the lower ferromagnetic transition temperature of the LTP, compared to that of the HTP. The ferromagnetic transition occurs within the LTP for $x = 0.00$ but within the HTP for $x = 0.05$. For these reasons, an anomalous enhancement of T_C between $x = 0.00$ and 0.05 is observed. When x is further increased, T_C monotonically decreases, as generally expected for a diluted magnetic system. Note that the ferromagnetic transition temperature for the LTP fragment in $x = 0.05$ (7 K) is the same as that in $x = 0.00$ (7 K), despite the increasing dilution ratio. The CTPT is suppressed in the vicinity of dopant Zn^{II} ions, and such vicinity can be considered as the HTP fragment. Therefore, the magnetic dilution does not affect the magnetic interaction in the LTP fragment. For this reason, T_C for the LTP fragment remains unchanged between $x = 0.00$ and $x = 0.05$.

It was previously reported that the transfer of electrons in the CTPT occurs within the magnetic honeycomb layer of $[\text{Fe}^{\text{II}}\text{Fe}^{\text{III}}(\text{dto})_3]^-$, as revealed by anisotropic resistivity measurement on $(n\text{-C}_3\text{H}_7)_4\text{N}[\text{Fe}^{\text{II}}\text{Fe}^{\text{III}}(\text{dto})_3]$ under high pressure.⁵² Moreover, the μSR measurement revealed that the nature of the CT in the CTPT is a dynamic oscillation of electrons between Fe^{II} and Fe^{III} sites with a frequency of 0.1 MHz under ambient pressure.⁴⁷ Considering these facts, a dielectric anomaly corresponding to the CTPT would be observed in the dielectric constant. Since the dielectric measurement possesses high signal detectability and fast responsiveness, we measured the temperature-dependent dielectric constant to elucidate the presence and disappearance of the CTPT in $(n\text{-C}_3\text{H}_7)_4\text{N}[\text{Fe}^{\text{II}}_{1-x}\text{Zn}^{\text{II}}_x\text{Fe}^{\text{III}}(\text{dto})_3]$. Figure 8

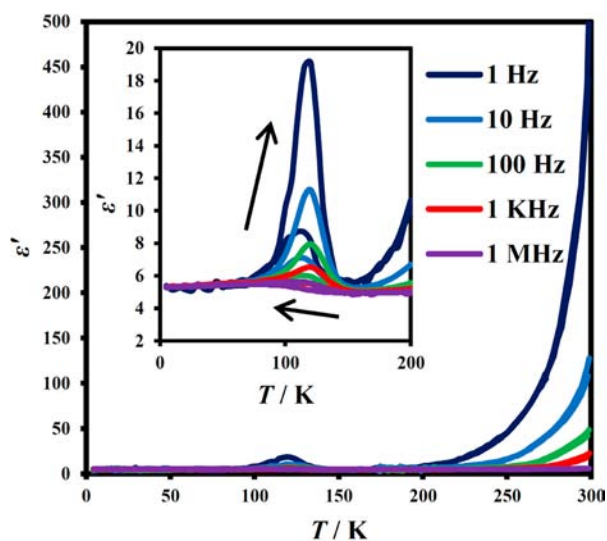


Figure 8. Temperature- and frequency-dependent dielectric constant (ϵ') of $x = 0.00$. Inset shows the low-temperature region.

shows the temperature dependence of the dielectric constant (ϵ') for $x = 0.00$ at several frequencies. Above 200 K, ϵ' remarkably depends on frequency and temperature, which is likely due to the thermal fluctuation of the counteranion, $(n\text{-C}_3\text{H}_7)_4\text{N}^+$. Moreover, an anomalous enhancement of ϵ' with a thermal hysteresis is observed at ~ 120 K across the entire measuring frequency range between 1 Hz and 1 MHz. As mentioned above, this observation can be attributed to the dynamic fluctuation of electrons between Fe^{II} and Fe^{III} sites associated with the CTPT. The anomaly becomes apparent as the frequency is lowered. Such frequency dependence is likely

to be caused by the slow relaxation of the electrons, due to the barrier of the electron hopping on the grain boundary of the compressed powder sample. These results clearly demonstrate that the CTPT is detectable by dielectric constant measurement. Figure 9 shows the temperature dependent dielectric

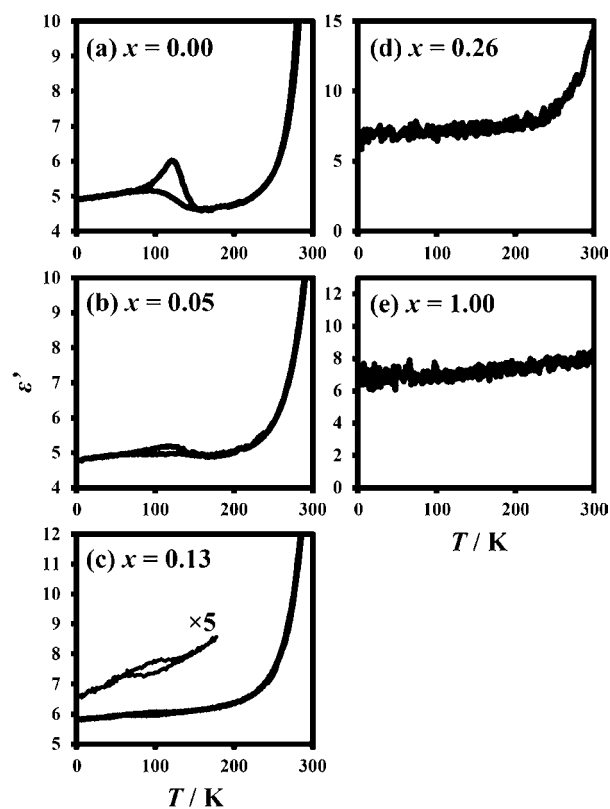


Figure 9. Temperature dependence of the dielectric constant (ϵ') for (a) $x = 0.00$, (b) $x = 0.05$, (c) $x = 0.13$, (d) $x = 0.26$, and (e) $x = 1.00$ measured at 1 kHz.

constant at 1 kHz for the selected samples ($x = 0.00, 0.05, 0.13, 0.26$, and 1.00) to clarify the characteristic Zn^{II} concentration dependence of the dielectric response of this series. The remaining data are shown in the Supporting Information (Figure S4). An anomalous enhancement of the dielectric constant with a large thermal hysteresis is observed for $x = 0.00$ and $x = 0.05$ (see Figures 9a and 9b), which almost disappears at $x = 0.13$, leaving only a small bump with a narrow hysteresis (Figure 9c). Both the upper and lower limits of the hysteresis are lowered with increasing Zn^{II} concentration. Above $x = 0.26$, the anomaly disappears from the dielectric constant (see Figures 9d and 9e). From these results, the critical Zn^{II} concentration for suppression of the CTPT is estimated at $x \approx 0.13$. Note that the anomalous behavior in the magnetic susceptibility associated with the CTPT is not observed for $x = 0.13$ (see Figure 3b). Furthermore, the spin configuration of the LTP fragment is not detected at 15 K for $x = 0.05$ and $x = 0.13$ in the Mössbauer study (see Figures S5 and S6 in the Supporting Information). These facts demonstrate that the dielectric measurement is a highly sensitive method to detect the CTPT.

On the basis of all of the above data, we present a phase diagram of the diluted magnetic system $(n\text{-C}_3\text{H}_7)_4\text{N}[\text{Fe}^{\text{II}}_{1-x}\text{Zn}^{\text{II}}_x\text{Fe}^{\text{III}}(\text{dto})_3]$ in Figure 10. In this diagram, $T_C(\text{HTP})$, $T_C(\text{LTP})$, $T_f(\text{CT})$, and $T_l(\text{CT})$ represent,

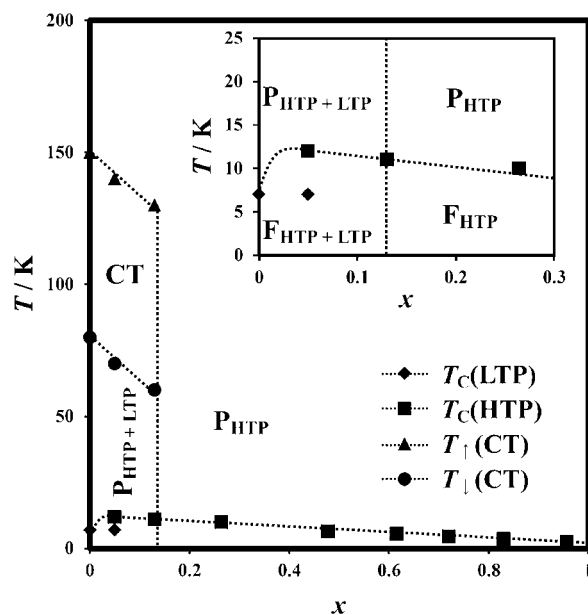


Figure 10. Phase diagram of $(n\text{-C}_3\text{H}_7)_4\text{N}[\text{Fe}^{\text{II}}_{1-x}\text{Zn}^{\text{II}}_x\text{Fe}^{\text{III}}(\text{dto})_3]$.

respectively, the ferromagnetic transition temperatures for the HTP and LTP, determined by the FCM, ZFCM, and RM measurements, and the upper and lower limits of the thermal hysteresis in the dielectric constant measured at 1 kHz, corresponding to the CTPT. At room temperature, the complex with Zn^{II} concentration $x = 0.00$ is a paramagnetic phase with the spin configuration of the HTP. This phase is denoted as P_{HTP} in the diagram. Below $T_{\uparrow}(\text{CT})$, the phase represented as CT appears at this concentration. In this phase, the CTPT occurs and the electrons dynamically oscillate between Fe^{II} and Fe^{III} . Below $T_{\downarrow}(\text{CT})$, a paramagnetic phase with the spin configuration of the LTP (denoted as P_{LTP}) appears, as a result of the CTPT. This complex exhibits a ferromagnetic transition at $T_{\text{C}}(\text{LTP})$, which results in a ferromagnetic phase with a spin configuration that remains in the LTP (denoted as F_{LTP}). The complexes in the Zn^{II} concentration region $0.00 < x \leq 0.13$ also exist in the P_{HTP} phase above $T_{\uparrow}(\text{CT})$, and the CT appears in the temperatures between $T_{\uparrow}(\text{CT})$ and $T_{\downarrow}(\text{CT})$. However, in contrast to $x = 0.00$, the CTPT for the complexes in this concentration region is partially suppressed, and, hence, the spin states at the temperatures below $T_{\downarrow}(\text{CT})$ are paramagnetic mixtures of the HTP and the LTP (denoted as $\text{P}_{\text{HTP}+\text{LTP}}$) down to the ferromagnetic transition temperature. As mentioned above, the ferromagnetic transitions for the complexes in this Zn^{II} concentration region occur at $T_{\text{C}}(\text{HTP})$ within the HTP domain. As a result, a ferromagnetic phase with a spin configuration in a mixture of the HTP and the LTP (denoted as $\text{F}_{\text{HTP}+\text{LTP}}$) appears below $T_{\text{C}}(\text{HTP})$. Note that this spin configuration is responsible for the two-stepped ferromagnetic transition in $x = 0.05$. For the complexes in the Zn^{II} concentration region of $x \geq 0.26$, the CTPT is completely suppressed and the CT disappears. Consequently, the complexes in this concentration region remain in P_{HTP} down to $T_{\text{C}}(\text{HTP})$ and exhibit ferromagnetic transitions at this temperature. This results in a ferromagnetic phase with the spin configuration of the HTP (F_{HTP}), except for in $x = 1.00$, where the ferromagnetic transition is not observed in any magnetic measurements within the examined temperature range.

As shown in the phase diagram, the critical concentration for the disappearance of the CTPT is unexpectedly low. Note that the significant Zn^{II} concentration dependence of the structure is not observed in the powder XRD patterns (see Figure 2). If this phase transition is not a cooperative phenomenon and the CT in the CTPT is accomplished only between a pair of Fe^{II} and Fe^{III} sites, the critical concentration is estimated at $x = 1.00$. From these facts, it is demonstrated that the CTPT is a highly cooperative phenomenon and the suppression of the CTPT by substituting Zn^{II} for Fe^{II} is related to the loss of cooperativity of the CT during the CTPT.

CONCLUSION

We have prepared a magnetically diluted series of complexes $(n\text{-C}_3\text{H}_7)_4\text{N}[\text{Fe}^{\text{II}}_{1-x}\text{Zn}^{\text{II}}_x\text{Fe}^{\text{III}}(\text{dto})_3]$ ($x = 0-1$) and investigated the effects of magnetic dilution on the charge-transfer phase transition (CTPT) and magnetic properties. These complexes are isostructural across the entire Zn^{II} concentration range. Magnetic and dielectric measurements reveal that the CTPT is gradually suppressed by substitution of Fe^{II} with Zn^{II} ions and finally disappears above a Zn^{II} concentration at $x \approx 0.13$. This unexpectedly low critical Zn^{II} concentration for the disappearance of the CTPT is indicative of high cooperativity of the electron transfers in the CTPT. In association with the gradual suppression of the CTPT, the spin state of the ferromagnetic state changes from the low-temperature phase (LTP) for $x = 0.00$ to a mixture of the LTP and high-temperature phase (HTP) for $0 < x \leq 0.13$ to the HTP for $x > 0.13$. Note that the spin configuration of the HTP gives a higher T_{C} value than that of the LTP. For these reasons, the ferromagnetic transition temperature T_{C} is enhanced by the substitution of Fe^{II} with Zn^{II} ions in the low Zn^{II} concentration region, despite the nonmagnetic nature of the Zn^{II} ion. Further increasing the substitution ratio causes a disconnection of the ferromagnetic exchange pathways between magnetic sites, which is accompanied by decreasing T_{C} ; finally, the ferromagnetic phase transition disappears in the very high Zn^{II} concentration region across the entire measured temperature range.

In the case of $x = 0.13$, the CTPT can be detected by means of dielectric constant measurement. However, no anomalous behavior associated with the CTPT is observed in the temperature-dependent magnetic susceptibility. Furthermore, the spin configuration of the LTP fragment could not be detected for the complexes with $x = 0.05$ and 0.13 in the Mössbauer spectra in the low-temperature region (i.e., at 15 K), because of the low signal-to-noise (SN) ratio of these spectra. These results demonstrate that dielectric measurement is a suitable method for the direct observation of a charge-transfer (CT) phenomenon in a mixed-valence complex, such as the CTPT.

ASSOCIATED CONTENT

Supporting Information

The remaining data of magnetic susceptibility, low-temperature magnetization, and dielectric constant; ac magnetic susceptibility for $x = 0.00$ and 0.05 ; ^{57}Fe Mössbauer spectra and parameters for $x = 0.05$ and 0.13 . This material is available free of charge via the Internet at <http://pubs.acs.org>.

AUTHOR INFORMATION

Corresponding Author

*E-mail: menomoto@rs.kagu.tus.ac.jp.

Notes

The authors declare no competing financial interest.

ACKNOWLEDGMENTS

This work was partially supported by a Grant-in-Aid for Young Scientists (No. 19750105) from the Ministry of Education, Culture, Sports, Science and Technology, Japan. We thank Dr. Y. Takahashi (Tokyo University of Science) for valuable discussions.

REFERENCES

- (1) Caneschi, A.; Gatteschi, D.; Sessoli, R.; Barra, A. L.; Brunel, L. C.; Guillot, M. *J. Am. Chem. Soc.* **1991**, *113*, 5873–5874.
- (2) Sessoli, R.; Gatteschi, D.; Caneschi, A.; Novak, M. A. *Nature* **1993**, *365*, 141–143.
- (3) Aubin, S. M. J.; Wemple, M. W.; Adams, D. M.; Tsai, H.; Christou, G.; Hendrickson, D. N. *J. Am. Chem. Soc.* **1996**, *118*, 7746–7754.
- (4) Gatteschi, D.; Sessoli, R. *Angew. Chem., Int. Ed.* **2003**, *42*, 268–297.
- (5) Caneschi, A.; Gatteschi, D.; Lalioti, N.; Sangregorio, C.; Sessoli, R.; Venturi, G.; Vindigni, A.; Rettori, A.; Pini, M.; Novak, M. A. *Angew. Chem., Int. Ed.* **2001**, *40*, 1760–1763.
- (6) Clérac, R.; Miyasaka, H.; Yamashita, M.; Coulon, C. *J. Am. Chem. Soc.* **2002**, *124*, 12837–12844.
- (7) Miyasaka, H.; Clérac, R. *Bull. Chem. Soc. Jpn.* **2005**, *78*, 1725–1748.
- (8) Bogani, L.; Vindigni, A.; Sessoli, R.; Gatteschi, D. *J. Mater. Chem.* **2008**, *18*, 4750–4758.
- (9) Coronado, E.; Galán-Mascarós, J. R.; Gómez-García, C. J.; Laukhin, V. *Nature* **2000**, *408*, 447–449.
- (10) Coronado, E.; Day, P. *Chem. Rev.* **2004**, *104*, 5419–5448.
- (11) Enoki, T.; Miyazaki, A. *Chem. Rev.* **2004**, *104*, 5449–5477.
- (12) Ōkawa, H.; Shigematsu, A.; Sadakiyo, M.; Miyagawa, T.; Yoneda, K.; Ohba, M.; Kitagawa, H. *J. Am. Chem. Soc.* **2009**, *131*, 13516–13522.
- (13) Ohkoshi, S.; Nakagawa, K.; Tomono, K.; Imoto, K.; Tsunobuchi, Y.; Tokoro, H. *J. Am. Chem. Soc.* **2010**, *132*, 6620–6621.
- (14) Pardo, E.; Train, C.; Gontard, G.; Boubekeur, K.; Fabelo, O.; Liu, H.; Dkhil, B.; Lloret, F.; Nakagawa, K.; Tokoro, H.; Ohkoshi, S.; Verdager, M. *J. Am. Chem. Soc.* **2011**, *133*, 15328–15331.
- (15) Kurmoo, M.; Graham, A. W.; Day, P.; Coles, S. J.; Hursthouse, M. B.; Caulfield, J. L.; Singleton, J.; Pratt, F. L.; Hayes, W.; Ducasse, L.; Guionneau, P. *J. Am. Chem. Soc.* **1995**, *117*, 12209–12217.
- (16) Coronado, E.; Martí-Gastaldo, C.; Navarro-Moratalla, E.; Ribera, A.; Blundell, S. J.; Baker, P. J. *Nat. Chem.* **2010**, *2*, 1031–1036.
- (17) Sato, O.; Iyoda, T.; Fujishima, A.; Hashimoto, K. *Science* **1996**, *272*, 704–705.
- (18) Shimizu, H.; Okubo, M.; Nakamoto, A.; Enomoto, M.; Kojima, N. *Inorg. Chem.* **2006**, *45*, 10240–10247.
- (19) Sato, O.; Tao, J.; Zhang, Y. *Angew. Chem., Int. Ed.* **2007**, *46*, 2152–2187.
- (20) Kida, N.; Hikita, M.; Kashima, I.; Okubo, M.; Itoi, M.; Enomoto, M.; Kato, K.; Tanaka, M.; Kojima, N. *J. Am. Chem. Soc.* **2009**, *131*, 212–220.
- (21) Ohkoshi, S.; Imoto, K.; Tsunobuchi, Y.; Takano, S.; Tokoro, H. *Nat. Chem.* **2011**, *3*, 564–569.
- (22) Clemente-León, M.; Coronado, E.; López-Jordà, M.; Desplanches, C.; Asthana, S.; Wang, H.; Létard, J. *Chem. Sci.* **2011**, *2*, 1121–1127.
- (23) Tamaki, H.; Zhong, Z. J.; Matsumoto, N.; Kida, S.; Koikawa, M.; Achiwa, N.; Hashimoto, Y.; Ōkawa, H. *J. Am. Chem. Soc.* **1992**, *114*, 6974–6979.
- (24) Clemente-León, M.; Coronado, E.; Martí-Gastaldo, C.; Romero, F. M. *Chem. Soc. Rev.* **2011**, *40*, 473–497.
- (25) Tamaki, H.; Mitsumi, M.; Nakamura, K.; Matsumoto, N.; Kida, S.; Ōkawa, H.; Iijima, S. *Chem. Lett.* **1992**, *21*, 1975–1978.
- (26) Mathonière, C.; Carling, S. G.; Yusheng, D.; Day, P. *J. Chem. Soc., Chem. Commun.* **1994**, 1551–1552.
- (27) Nuttall, C. J.; Bellitto, C.; Day, P. *J. Chem. Soc., Chem. Commun.* **1995**, 1513–1514.
- (28) Pellaux, R.; Schmalle, H. W.; Huber, R.; Fischer, P.; Hauss, T.; Ouladdiaf, B.; Decurtins, S. *Inorg. Chem.* **1997**, *36*, 2301–2308.
- (29) Larionova, J.; Mombelli, B.; Sanchiz, J.; Kahn, O. *Inorg. Chem.* **1998**, *37*, 679–684.
- (30) Clemente-León, M.; Coronado, E.; Galán-Mascarós, J. R.; Gómez-García, C. J. *Chem. Commun.* **1997**, 1727–1728.
- (31) Coronado, E.; Galán-Mascarós, J.; Gómez-García, C. J.; Ensling, J.; Gütllich, P. *Chem.—Eur. J.* **2000**, *6*, 552–563.
- (32) Coronado, E.; Giménez-Saiz, C.; Gómez-García, C. J.; Romero, F. M.; Tarazón, A. *J. Mat. Chem.* **2008**, *18*, 929–934.
- (33) Bénard, S.; Rivière, E.; Yu, P.; Nakatani, K.; Delouis, J. F. *Chem. Mater.* **2001**, *13*, 159–162.
- (34) Alberola, A.; Coronado, E.; Galán-Mascarós, J. R.; Giménez-Saiz, C.; Gómez-García, C. J. *J. Am. Chem. Soc.* **2003**, *125*, 10774–10775.
- (35) Coronado, E.; Galán-Mascarós, J. R.; Gómez-García, C. J.; Martínez-Ferrero, E.; van Smaalen, S. *Inorg. Chem.* **2004**, *43*, 4808–4810.
- (36) Bénard, S.; Yu, P.; Coradin, T.; Rivière, E.; Nakatani, K.; Clément, R. *Adv. Mater.* **1997**, *7*, 981–984.
- (37) Bénard, S.; Yu, P.; Audière, J. P.; Rivière, E.; Clément, R.; Guilhem, J.; Tehertanov, L.; Nakatani, K. *J. Am. Chem. Soc.* **2000**, *122*, 9444–9454.
- (38) Lacroix, P. G.; Malfant, I.; Bénard, S.; Yu, P.; Rivière, E.; Nakatani, K. *Chem. Mater.* **2001**, *13*, 441–449.
- (39) Endo, T.; Akutagawa, T.; Noro, S.; Nakamura, T. *Dalton Trans.* **2011**, *40*, 1491–1496.
- (40) Ōkawa, H.; Mitsumi, M.; Ohba, M.; Kōdera, M.; Matsumoto, N. *Bull. Chem. Soc. Jpn.* **1994**, *67*, 2139–2144.
- (41) Kojima, N.; Aoki, W.; Itoi, M.; Ono, Y.; Seto, M.; Kobayashi, Y.; Maeda, Y. *Solid State Commun.* **2001**, *120*, 165–170.
- (42) Nakamoto, T.; Miyazaki, Y.; Itoi, M.; Ono, Y.; Kojima, N.; Sorai, M. *Angew. Chem., Int. Ed.* **2001**, *40*, 4716–4719.
- (43) Itoi, M.; Taira, A.; Enomoto, M.; Matsushita, N.; Kojima, N.; Kobayashi, Y.; Asai, K.; Koyama, K.; Nakano, T.; Uwatoko, Y.; Yamamura, J. *Solid State Commun.* **2004**, *130*, 415–420.
- (44) Itoi, M.; Ono, Y.; Kojima, N.; Kato, K.; Osaka, K.; Takata, M. *Eur. J. Inorg. Chem.* **2006**, 1198–1207.
- (45) Mochida, T. *Mol. Cryst. Liq. Cryst.* **2000**, *343*, 205–210.
- (46) Mochida, T.; Takazawa, K.; Matsui, H.; Takahashi, M.; Takeda, M.; Sato, M.; Nishio, Y.; Kajita, K.; Mori, H. *Inorg. Chem.* **2005**, *44*, 8628–8641.
- (47) Kida, N.; Enomoto, M.; Watanabe, I.; Suzuki, T.; Kojima, N. *Phys. Rev. B* **2008**, *77*, 144427.
- (48) Enomoto, M.; Kojima, N. *Polyhedron* **2009**, *28*, 1826–1829.
- (49) Dwyer, F. P.; Sargeson, A. M. *J. Am. Chem. Soc.* **1959**, *81*, 2335–2336.
- (50) Ono, Y.; Okubo, M.; Kojima, N. *Solid State Commun.* **2003**, *126*, 291–296.
- (51) Mayoh, B.; Day, P. *J. Chem. Soc., Dalton Trans.* **1976**, 1483–1486.
- (52) Enomoto, M.; Itoi, M.; Ono, Y.; Okubo, M.; Kojima, N. *Synth. Met.* **2003**, *137*, 1231–1232.